Journal of the Korean Astronomical Society
52: 109 ∼ 119, 2019 August
https://doi.org/10.5303/JKAS.2019.52.4.109
pISSN: 1225-4614 · eISSN: 2288-890X
http://jkas.kas.org

Seoul National University AGN Monitoring Project. I. Strategy And Sample

Jong-Hak Woo[1], Donghoon Son[1], Elena Gallo[2], Edmund Hodges-Kluck[2,3], Yiseul Jeon[1], Jaejin Shin[1], Hyun-Jin Bae[1], Hojin Cho[1], Wanjin Cho[1], Daeun Kang[1], Wonseok Kang[6], Marios Karouzos[1], Minjin Kim[4], Taewoo Kim[6], Huynh Anh N. Le[1], Daeseong Park[5], Songyoun Park[1], Suvendu Rakshit[1], and Hyun-il Sung[5]

[1]Astronomy Program, Department of Physics and Astronomy, Seoul National University, Seoul 08826, Korea; woo@astro.snu.ac.kr
[2]Department of Astronomy, University of Michigan, Ann Arbor, MI 48109, USA
[3]NASA/GSFC, Code 662, Greenbelt, MD 20771, USA
[4]Department of Astronomy and Atmospheric Sciences, Kyungpook National University, Daegu 41566, Korea
[5]Korea Astronomy and Space Science Institute, 776 Daedeok-daero, Yuseong-gu, Daejeon 34055, Korea
[6]National Youth Space Center, Goheung, Jeollanam-do 59567, Korea

Received March 27, 2019; accepted June 13, 2019

Abstract: While the reverberation mapping technique is the best available method for measuring black hole mass in active galactic nuclei (AGNs) beyond the local volume, this method has been mainly applied to relatively low-to-moderate luminosity AGNs at low redshift. We present the strategy of the Seoul National University AGN Monitoring Project, which aims at measuring the time delay of the Hβ line emission with respect to AGN continuum, using a sample of relatively high luminosity AGNs out to redshift $z \sim 0.5$. We present simulated cross correlation results based on a number of mock light curves, in order to optimally determine monitoring duration and cadence. We describe our campaign strategy based on the simulation results and the availability of observing facilities. We present the sample selection, and the properties of the selected 100 AGNs, including the optical luminosity, expected time lag, black hole mass, and Eddington ratio.

Key words: galaxies: active — galaxies: nuclei — galaxies: Seyfert

1. Introduction

Black hole mass ($M_{\rm BH}$) is a key parameter in understanding the physics of active galactic nuclei (AGNs). The correlation of $M_{\rm BH}$ with the global properties of host galaxies observed in inactive (e.g., Ferrarese & Merritt 2000; Gebhardt et al. 2000; Kormendy & Ho 2013) and active galaxies (e.g., Woo et al. 2013; Grier et al. 2013; Woo et al. 2015) are often interpreted as a strong connection between black hole growth and galaxy evolution (see Kormendy & Ho 2013). To investigate the physics of AGN phenomena (e.g., Woo & Urry 2002; Kollmeier et al. 2006; Davis et al. 2007; Bentz et al. 2013; Woo et al. 2016), $M_{\rm BH}$ must be accurately determined. Dynamical methods based on high angular resolution data are a common approach to measure $M_{\rm BH}$ (e.g., Kormendy & Ho 2013). However, owing to the small scale of the sphere of the influence of typical supermassive black holes, the dynamical method is limited to galaxies within a distance of ∼100 Mpc using current technology.

Reverberation mapping is the best available method to determine $M_{\rm BH}$ beyond the local volume. Based on the virial assumption that the kinematics of gas in the broad-line region (BLR) is governed by the black hole's gravity, $M_{\rm BH}$ can be determined by measuring the size and velocity of the BLR gas. The geometry and kinematics of the BLR gas can be mapped in the time domain with the reverberation mapping technique (Blandford & McKee 1982; Peterson 1993) using the relation $M_{\rm BH} \propto R_{\rm BLR}V^2$, where $R_{\rm BLR}$ is the measured time lag (i.e., the light travel time) between AGN continuum region and BLR gas, while V is velocity measured from the width of the broad-emission lines. Previous reverberation studies showed that the size (time lag) and velocity of the Hβ emission line measured at different epochs clearly followed the virial relation, indicating that the virial assumption is valid (Peterson et al. 2004), while measurements of the black hole mass suffer from systematic uncertainties due to the complex nature of the BLR kinematics (Park et al. 2012; Bentz et al. 2010; Pancoast et al. 2014).

More than 60 masses have been reliably measured using this method (e.g., Wandel et al. 1999; Kaspi et al. 2000; Peterson et al. 2004; Bentz et al. 2009; Barth et al. 2011; Grier et al. 2013; Barth et al. 2015; Fausnaugh et al. 2017; Park et al. 2017). However, due to observational challenges, this method has been mainly applied to relatively low-to-moderate luminosity AGNs at low redshift. As a long-term spectroscopic monitoring campaign is required for reliable lag measurements, it is difficult to increase the sample size.

Nevertheless, recent reverberation campaigns have

Corresponding author: J.-H. Woo

achieved significant progress by increasing the size and dynamic range of the sample. For example, the Lick AGN Monitoring Project 2008, 2011 utilized the 3-m aperture Lick telescope to carry out semi-consecutive nightly observations over 2–3 months, respectively, in 2008 and 2011. This program was the first dedicated reverberation mapping project using a mid-size telescope (Barth et al. 2015). Other studies targeted high Eddington ratio AGNs for investigating the photoionization and validity of indirect mass estimators (Du et al. 2015, 2016). Based on a very long-term campaign, a number of lag measurements using the rest-frame UV lines has been also reported for high-z AGNs (Lira et al. 2018). Recently, a new approach has been applied with a multi-object spectrograph, for simultaneously monitoring multiple AGNs. For example, the SDSS-reverberation mapping project, monitoring hundreds of AGNs out to $z \sim 4.5$, was carried out over six months (Shen et al. 2016; Grier et al. 2017). Also, as a part of the Australian spectroscopic dark energy survey (OzDES), a multi-object reverberation program is underway for monitoring hundreds of quasars.

Reverberation mapping data are of paramount importance since they provide the fundamental calibration for all indirect $M_{\rm BH}$ estimators, which in turn enable us to investigate black hole growth and accretion physics over cosmic time. However, the reverberation mapping method is still limited to a relatively small number of local AGNs, while numerous AGNs are detected out to $z \sim 7$. The main limitation of current reverberation studies is the lack of high-luminosity and high-redshift AGNs in the sample. The majority of the Hβ reverberation-mapped sample are low-to-intermediate luminosity AGNs, predominantly located at $z \lesssim 0.1$. The bias toward low luminosity AGNs is a natural consequence of the lack of long-term monitoring programs, as several years of spectroscopic observations are required to measure large time lags (i.e, $>$ 100 days in the rest frame). In addition, time dilation due to Hubble expansion increases the observed lag of high-z AGNs by a factor of $(1+z)$. Thus, very long monitoring is required for reverberation mapping of high-z AGNs (e.g., Lira et al. 2018). So far, the longest observed Hβ lag is ∼300 days in the rest frame.

The luminosity limitation of the current reverberation-mapped AGN sample can seriously bias the empirical size-luminosity relation (Bentz et al. 2006), which is mainly used to estimate $M_{\rm BH}$ of a large number of AGNs. Thus, a major effort to obtain relatively long lag measurements using luminous AGNs is necessary to overcome the current limitation of $M_{\rm BH}$ studies. In this paper, we present the Seoul National University AGN monitoring project, which aims at measuring Hβ time lag of relatively high luminosity AGNs at $z < 0.5$. The strategy of the project and the simulation results are presented in Section 2 and Section 3, respectively. The sample selection and sample properties are presented in Section 4. We summarize in Section 5.

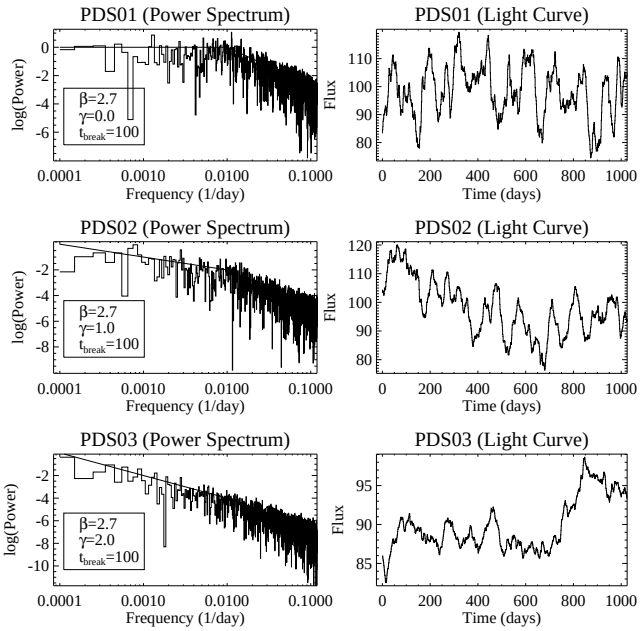

Figure 1. Examples of power density spectra generated with a broken power law (left) and the corresponding light curves (right). The three parameters, β, γ, and $t_{\rm break}$ are specified alongside each power spectrum. The light curves are normalized to an r.m.s. amplitude of 10%.

2. PROJECT STRATEGY

High-luminosity AGNs will be the most important targets to overcome the current limitation of Hβ reverberation studies. Since the expected time lag of high luminosity AGNs is very long, and made longer by the time dilation effect due to redshift, several years of monitoring is required as a minimum. At the same time, a relatively large aperture telescope is needed to measure the flux variation of the Hβ emission line of these faint AGNs at cosmological distances.

To set up a long-term monitoring project, we consider three factors: expected lags, monitoring duration and cadence, which are the key parameters for a successful campaign. The expected lag depends on the luminosity of each target and can be estimated from the size-luminosity relation (Bentz et al. 2006). We select a sample of relatively high luminosity AGNs with a monochromatic luminosity at 5100 Å of $L_{5100} \sim 10^{44-46}$ erg s^{-1}, in order to cover the high-luminosity end of the size-luminosity relation. The Hβ lag of these AGNs is expected to be more than ∼100 days in the observer frame. Based on a three year monitoring program, we expect to measure Hβ time lags up to ∼300 days, by considering that the monitoring length has to be longer than the expected lag by a factor of 3–5. Thus, we aim at measuring Hβ lags of 100–400 days in the observer frame. In terms of cadence, it is desirable to have a factor of 5 or better time resolution for a given time lag, as implemented in previous studies. Thus, a ∼20 day cadence is required to measure a 100 day time lag.

Considering these conditions, we initially design a

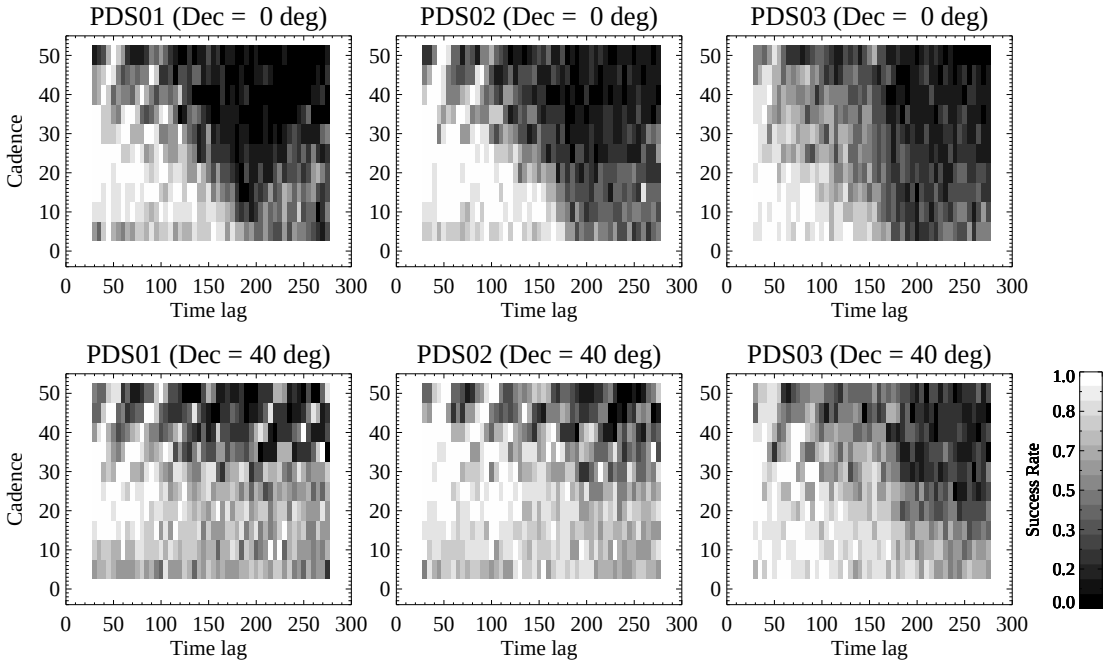

Figure 2. The estimated success rate maps of three PDSs as a function of cadence and time lag for the three year campaign duration. We assumed two different seasonal gaps (i.e., Dec = 0° and 40°). The colors indicate success rates from 0% (black) to 100% (white).

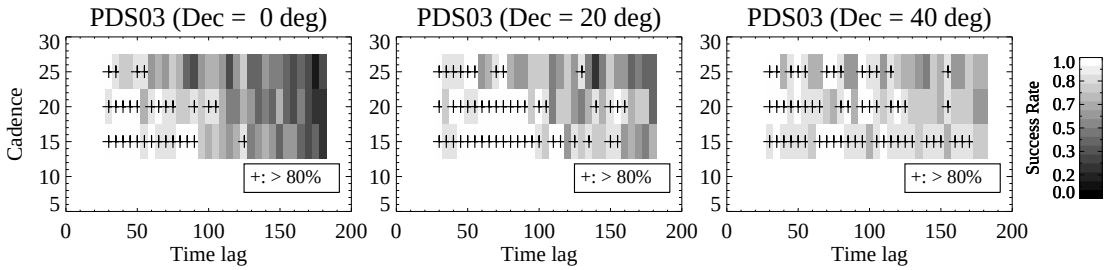

Figure 3. Simulated success rate maps for three declination values (i.e., Dec = 0°, 20°, and 40°) for the case of PDS03 and a campaign duration of three years. Plus signs indicate combinations of cadence and time lag that provide success rates greater than 80%. The colors indicate success rates from 0% (black) to 100% (white).

three year monitoring program, which is also limited by funding and availability of observing facilities. For spectroscopy, we need ∼20 nights per year of a mid-size telescope in order to obtain good quality spectra. With a 20–30 day cadence, a total of ∼50–60 epochs of spectroscopic data can be obtained during a three year campaign. In the case of photometry, we can achieve a higher time resolution, i.e., a 10 day cadence since photometry can be accurately performed with smaller telescopes, which are much easier to access.

3. Simulation Results

To quantify the best strategy for the monitoring program, we simulate the success rate as a function of time lag, campaign duration, and cadence. We generate continuum and line emission light curves to perform cross-correlation analysis (Section 3.2). While it is clear that a shorter cadence and longer campaign duration can increase the success rate, we need to investigate optimal criteria of cadence and duration since observing facilities are limited. By comparing the input lag, which is used to delay an emission line light curve with respect to a continuum light curve, with the measured lag based on the cross-correlation analysis, we determine whether the lag measurement is successful. The simulation is conducted with various cadences and campaign durations to calculate the success rate for each case (Section 3.3). After identification of optimal criteria which satisfy success rates ≥80%, we select the sample accordingly (Section 4.1).

3.1. Generating Light Curves

We simulate a continuum light curve by generating mock light curves with lengths ranging from one to five years, using a power density spectrum (PDS). Then, we delay the continuum light curve by a specific time lag, in order to define an emission-line light curve. These two light curves are sampled with a given cadence (e.g.,

60 epochs for three years).

For generating mock light curves, we use the method described by Timmer & König (1995). The variability of AGN can be described as a $1/f$ fluctuation (Lawrence et al. 1988), meaning that the spectral power scales as $1/f$ with f being the frequency. From Kepler data (Barth, A., private communication), the slopes of PDS for the high frequency region are -2.5 to -3.0. However, if we apply this steep slope to low frequencies, the generated light curves show very strong secular trends which do not reflect actual AGN light curves. To create light curves that are relatively flat on long time scales (i.e., low frequencies), we use PSDs that follow broken power laws of the form $P(f) \propto f^{-\beta}$ for $f > 1/t_{\rm break}$ and $P(f) \propto f^{-\gamma}$ for $f < 1/t_{\rm break}$; here, the frequency f is in units of day^{-1}, β is the power law index for the high frequency region, γ is the power law index for the low frequency region, and $t_{\rm break}$ is the break time scale. We fix β to -2.7, i.e. in the middle of the range suggested by the Kepler data. We test various γ values to control the long-term shapes of light curves and select three values, $\gamma = 0, 1, 2$. We fix t_{break} to 100 days as this value produces the most realistic light curves for our selected values of γ. In the following, we refer to three cases of different PDSs as PDS01, PDS02, and PDS03 with $\gamma = 0$, 1, and 2, respectively; they are presented in Figure 1 (left panels).

Using the selected parameter values, we generate power spectra with a sampling interval of one day then add randomized Fourier amplitudes to each spectrum. Then, via Fourier transformation, we create a series of light curves as shown in Figure 1 (right panels). Note that as the value of γ increases, the spectral power at low frequencies (i.e., long-term variations of the light curves) gets stronger and the secular trends get weaker.

For the continuum light curves, we normalize the variability amplitude by adopting a typical value. AGN variability studies show that the r.m.s. amplitude in the optical continuum is ∼10–20%. In this simulation we adopt a conservative value of 10%. For the emission-line light curves, we assume for simplicity that the amplitude of variability is the same as in the continuum. After sampling the continuum and the emission line light curves with a specific cadence, we assign relative errors of 1% to the continuum flux values and of 2% to the emission line flux values.

For each target, there will be a seasonal gap when it is not observable at night. The length of the seasonal gap is a function of declination of each target for a given ground-based telescope. For example, at the Lick observatory, located at a latitude of $+37°{:}20'{:}36''$, the maximum number of observation nights with airmasses < 2 is 180, 212, 238, and 266 days per year, respectively, for a target declination of 0°, 20°, 40°, and 60°. Thus, if we select targets at Dec $> 40°$, seasonal gaps will be shorter than four months.

3.2. Time Lag Measurement

To measure a time lag, we generate a series of two light curves (continuum and emission line fluxes, respectively) using a set of four parameters. First. we use three different PDSs as presented in Figure 2. Second, we choose an intrinsic time lag between 30 and 275 days. Third, we fix the monitoring cadence to a value between 5 and 50 days. Fourth, we determine a seasonal gap using one out of three different declinations (0°, 20°, and 40°). To measure the time lag of an emission line light curve with respect to a continuum light curve, we utilize the software JAVELIN which measures time lags between two light curves by adopting a damped random walk to model AGN variability (Zu et al. 2011, 2013). For each set of parameters, we use 10 random light curves to measure time lags and calculate the success rate. To decide whether the measured time lag agrees with the intrinsic time lag, we consider the measurement as a success if the relative difference between the measured and intrinsic lags is less than 10%.

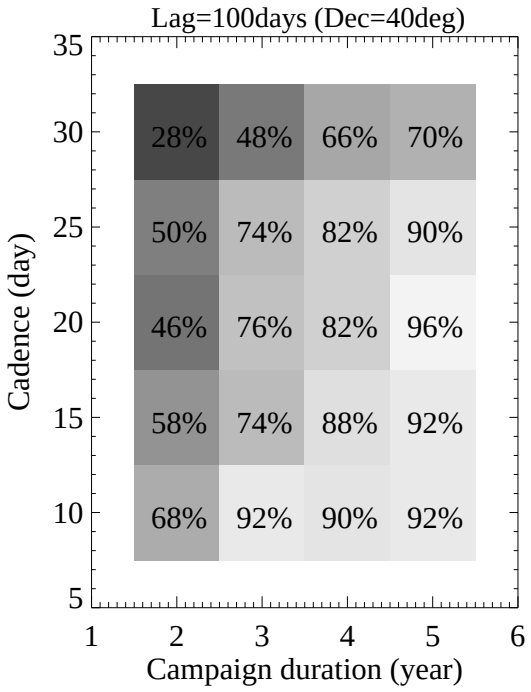

Figure 4. Success rates as function of cadence and campaign duration for a specific target with an expected time lag of 100 days and located at a declination of 40°. The number in each box indicates the success rate in %.

3.3. Success Rates

We present the success rates for a three-year campaign, as function of cadence and time lag, in Figure 2. Accounting for the impact of seasonal gaps, we show results for declinations of 0° and 40°, respectively. As expected, the light curves generated from a conservative power density spectrum PDS03 (i.e., $\gamma = 2.0$, highest power at lowest frequencies) generally show lower success rates than those from other PDSs with smaller γ values. Shorter seasonal gaps (i.e., declination 40°) translate into higher success rates. Notably, intrinsic time lags coinciding with the lengths of seasonal gaps (e.g., a target with a ∼180 day lag at declination 0°)

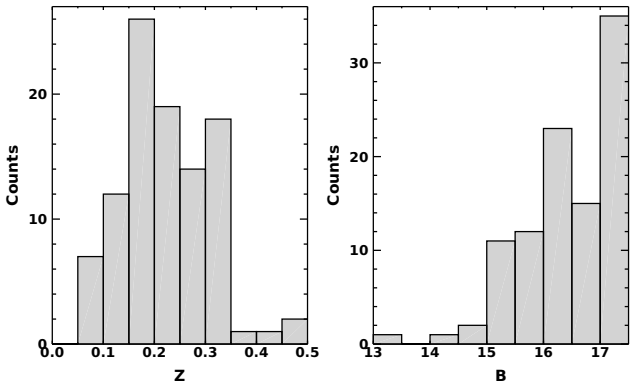

Figure 5. Distributions of redshift (left) and apparent B-band magnitude (right) of the sample.

cause the success rate to drop to almost 0% regardless of the cadence (see top left panel in Figure 2).

In Figure 3, we mark combinations of intrinsic time lag and cadence for which the success rate is larger than 80%, focusing on the case of PDS03 (the most conservative case). If we adopt a 15-day cadence for a three-year monitoring program, intrinsic time lags of 30–150 days can be measured with a 80% success rate for AGNs at declinations $> 20°$. If the cadence is 20 days, we can still measure intrinsic time lags between 30 and 130 days for AGNs at declinations $> 40°$.

To investigate how the campaign duration affects the success rate, we present the success rate as a function of cadence and campaign duration, using the PDS03 light curves, a fixed intrinsic time lag of 100 days and a declination of 40°, in Figure 4. For this simulation, we generate 50 sets of light curves for each bin (combination of cadence and campaign duration), and measure the time lag in each case. The number in each map cell indicates the success rate. For example, in the case of a 20 day cadence, we obtain a success rate of 76% for a three-year campaign, while the success rate increases to 96% if the campaign duration is extended to five years.

Based on these results, we conclude that a three-year monitoring campaign with a 20 day cadence can provide high quality lag measurements with errors within 10% and with a 80% success rate for AGNs with intrinsic time lag ∼150 days. Note that the simulated results are based on idealized light curves and there could be various other effects that could decrease the success rate. Here we take these results as a guideline for preparing a reasonable monitoring campaign. We decide to perform a three-year monitoring campaign with cadences of ∼20 days for spectroscopy and ∼10 days for photometry.

4. Sample

4.1. Sample Selection

We use the MILLIQUAS Catalog to select AGNs at $z < 0.5$ and with V-band magnitudes < 17. The expected lags are estimated from the optical luminosity at 5100 Å, based on the size-luminosity relation

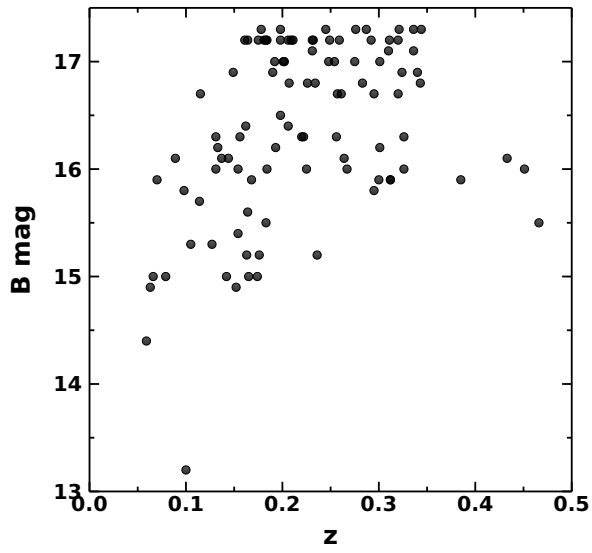

Figure 6. Apparent B-band magnitude as function of redshift redshifts for the AGNs in our sample.

(Bentz et al. 2013). Using available spectra from various archives, we perform spectral decomposition to separate the power-law continuum, Fe II emission, and stellar component. Then, we measure the rest-frame luminosity at 5100 Å (L_{5100}) from the power-law component. For 11 AGNs for which no archival spectrum is available, we use spectra obtained at the Lick 3-m or MDM 2.4-m telescopes during our initial spectroscopy test. Details of our spectroscopic observations are summarized by Rakshit et al. (2019).

As a primary sample, we select 48 AGNs at declinations $> 20°$ and expected observer-frame time lags $70 < (1 + z)\tau < 250$ days. Considering the large uncertainties in the estimated time lags, we also select 37 AGNs with shorter lags $40 < (1 + z)\tau < 70$ days. We refer to these two groups as primary 1 (Pr1) and primary 2 (Pr2) groups; they are presented in Tables 1 and 2, respectively. In addition, we choose a sample of 15 AGNs (presented in Table 3) from the Palomar Green quasar catalogue with a lower declination limit of $> 0°$, in order to increase the sample size. Thus, a total of 100 AGNs at $z < 0.5$ are selected for initial imaging and spectroscopy, to examine the number of comparison stars in the fields of view and the shapes of the Hβ and [OIII] emission lines, and for a feasibility test of differential photometry and spectral decomposition.

4.2. Sample Properties

In Figure 5, we present the redshift distribution of the sample; the mean redshift is 0.22 ± 0.09. We limit the redshift to $z \sim 0.5$ in order to properly locate the Hβ emission line within the spectral range of the optical spectral setup. Thus, we can avoid a change of the grating or tilt angle of the spectrograph during the observing runs, thus minimizing overheads and systematic uncertainties. For high-z AGNs, the factor $(1 + z)$ increases the time lag in the observer frame by over 50% at $z > 0.5$.

Table 1
Properties of the AGNs in our Primary 1 sample

Name	RA	Dec	z	B	$(1+z)\tau$ (day)	$\log L_{5100,\mathrm{spec}}$ (erg s^{-1})	$(1+z)\tau_{\mathrm{spec}}$ (day)	$\log M_{\mathrm{BH}}$ ($M_\odot$)	Ref. Spec.
(1)	(2)	(3)	(4)	(5)	(6)	(7)	(8)	(9)	(10)
Pr1_ID01	01:01:31.1	+42:29:36.0	0.190	16.9	84.7	44.6	87.8	8.82	Lick
Pr1_ID02	01:04:15.8	+40:22:44.0	0.193	16.2	121.2	45.1	149.3	8.51	Lick
Pr1_ID03	01:40:35.0	+23:44:51.0	0.320	16.7	186.7	45.0	155.3	8.49	Lick
Pr1_ID04	02:27:39.7	+44:10:00.0	0.175	17.2	65.4	44.0	40.5	7.65	Lick
Pr1_ID05	02:28:59.2	+39:08:44.0	0.336	17.1	165.1	44.3	67.7	†	MDM
Pr1_ID06	03:37:02.9	+47:38:50.0	0.184	17.2	70.1	44.9	113.1	8.43	Lick
Pr1_ID07	04:13:37.6	+72:06:52.7	0.105	15.3	88.9	44.1	44.2	7.86	MDM
Pr1_ID08	07:46:44.8	+29:40:59.0	0.292	17.2	128.0	44.5	81.3	7.98	SDSS
Pr1_ID09	07:49:10.6	+28:42:14.6	0.344	17.3	156.2	44.8	119.3	8.81	SDSS
Pr1_ID10	07:56:20.1	+30:45:35.4	0.236	15.2	258.9	44.8	105.7	8.44	SDSS
Pr1_ID11	08:01:12.0	+51:28:12.3	0.321	17.3	140.9	44.2	59.7	7.99	SDSS
Pr1_ID12	08:16:52.9	+24:16:12.6	0.276	17.3	113.2	44.6	90.8	8.30	SDSS
Pr1_ID13	09:28:01.3	+49:18:17.3	0.115	16.7	49.8	43.7	25.3	7.29	SDSS
Pr1_ID14	09:39:39.7	+37:57:05.8	0.231	17.2	94.3	44.5	72.0	8.24	SDSS
Pr1_ID15	09:50:48.4	+39:26:50.5	0.206	16.4	119.5	44.6	81.7	8.76	SDSS
Pr1_ID16	10:05:28.3	+42:30:37.6	0.257	16.7	137.4	44.8	108.8	8.53	SDSS
Pr1_ID17	10:26:13.9	+52:37:51.3	0.259	17.2	109.0	44.3	64.3	8.30	SDSS
Pr1_ID18	10:59:35.5	+66:57:58.0	0.340	16.9	187.2	44.8	117.4	8.67	SDSS
Pr1_ID19	11:04:13.9	+76:58:58.2	0.312	15.9	271.5	45.1	172.4	9.34	SDSS
Pr1_ID20	11:05:27.3	+67:16:36.4	0.320	17.2	146.1	44.6	96.2	8.76	SDSS
Pr1_ID21	11:15:06.0	+42:49:48.9	0.301	16.2	218.5	44.9	130.5	8.63	Lick
Pr1_ID22	11:19:08.7	+21:19:18.0	0.176	15.2	179.1	45.1	147.1	8.71	SDSS
Pr1_ID23	11:20:07.4	+42:35:51.4	0.226	16.8	111.5	44.4	70.8	8.77	SDSS
Pr1_ID24	11:24:39.2	+42:01:45.1	0.225	16.0	161.0	44.9	119.9	8.36	SDSS
Pr1_ID25	11:34:32.2	+60:46:34.8	0.201	17.0	86.5	44.2	48.6	8.51	SDSS
Pr1_ID26	12:03:48.1	+45:59:51.1	0.343	16.8	197.1	44.9	143.3	8.88	SDSS
Pr1_ID27	12:04:42.1	+27:54:11.8	0.165	15.0	177.4	44.5	72.4	9.02	SDSS
Pr1_ID28	12:07:21.0	+26:24:29.2	0.324	16.9	174.0	45.0	155.8	8.49	SDSS
Pr1_ID29	12:17:52.2	+33:34:47.3	0.178	17.3	64.0	44.4	64.0	8.64	SDSS
Pr1_ID30	12:53:37.7	+21:26:18.2	0.127	15.3	111.7	44.4	63.5	8.77	SDSS
Pr1_ID31	13:12:17.8	+35:15:21.1	0.183	15.5	163.3	44.7	97.5	8.57	SDSS
Pr1_ID32	13:56:32.8	+21:03:52.4	0.300	15.9	259.3	45.1	166.7	8.78	SDSS
Pr1_ID33	14:03:08.8	+37:58:27.5	0.184	16.0	126.3	44.5	69.2	8.23	SDSS
Pr1_ID34	14:08:39.0	+63:06:00.5	0.261	16.7	141.3	44.7	103.9	8.67	SDSS
Pr1_ID35	14:08:54.2	+56:57:43.4	0.336	17.3	149.7	44.9	137.4	8.79	SDSS
Pr1_ID36	14:15:35.9	+48:35:43.6	0.275	17.0	131.1	44.5	83.2	8.46	SDSS
Pr1_ID37	14:46:45.9	+40:35:05.8	0.267	16.0	210.2	45.1	164.5	8.44	SDSS
Pr1_ID38	14:56:08.6	+38:00:38.6	0.283	16.8	149.1	44.6	84.8	9.09	SDSS
Pr1_ID39	15:15:35.3	+48:05:30.6	0.312	15.9	268.2	45.1	178.9	8.75	SDSS
Pr1_ID40	15:26:24.0	+27:54:52.1	0.231	17.1	99.0	44.7	94.3	8.58	SDSS
Pr1_ID41	15:40:04.3	+35:50:50.1	0.164	17.2	60.2	44.2	51.3	8.08	SDSS
Pr1_ID42	15:47:43.5	+20:52:16.8	0.264	16.1	197.2	45.0	139.9	9.11	SDSS
Pr1_ID43	16:19:11.2	+50:11:09.2	0.234	16.8	116.4	44.4	63.8	8.69	SDSS
Pr1_ID44	16:46:49.1	+38:25:04.6	0.311	17.2	141.6	44.7	102.9	7.93	SDSS
Pr1_ID45	17:12:06.3	+58:42:17.0	0.310	17.1	146.8	44.8	121.0	†	Lick
Pr1_ID46	17:14:48.5	+33:27:38.3	0.181	17.2	68.2	44.4	64.9	8.84	SDSS
Pr1_ID47	19:35:21.2	+53:14:12.1	0.248	17.0	113.5	45.0	146.9	8.64	Lick
Pr1_ID48	23:03:29.9	+45:37:40.6	0.301	17.0	147.6	44.7	99.6	8.91	MDM

Columns: (1) Target ID. (2) RA in J2000.0. (3) Dec in J2000.0. (4) Redshift. (5) Apparent B-band magnitude from the literature. (6) Observer-frame time lag $(1+z)\tau$ in days, estimated from the B-band magnitude in column (5). (7) L_{5100} measured from a reference spectrum. (8) $(1+z)\tau$ value measured using column (7) and Equation (3). (9) Black hole mass estimated using Equation (4) using the velocity dispersion (σ) of a broad Hβ emission line and L_{5100} in column (7). † Pr1_ID05 and Pr1_ID45: no Hβ line was detected. (10) References for individual spectra: SDSS – SDSS DR12 archive, Lick or MDM – obtained with our program.

The distribution of the apparent B-band magnitude is presented in Figure 5 (right panel), ranging from $B = 13.2$ to $B = 17.3$, with a mean $\langle B \rangle = 16.3 \pm 0.8$. Note that the B-band magnitude is obtained from various catalogues in the literature. Thus, we expect that the current B-band magnitude will be somewhat different due to variability over time. We compare the distributions of redshift and B-band magnitude in Figure 6,

Table 2
Properties of the AGNs in our Primary 2 sample

Name	RA	Dec	z	B	$(1+z)\tau$ (day)	$\log L_{5100,\mathrm{spec}}$ (erg s^{-1})	$(1+z)\tau_{\mathrm{spec}}$ (day)	$\log M_{\mathrm{BH}}$ ($M_\odot$)	Ref. Spec.
(1)	(2)	(3)	(4)	(5)	(6)	(7)	(8)	(9)	(10)
Pr2_ID01	08:03:08.6	+53:00:04.8	0.287	17.3	119.9	44.3	58.9	8.24	SDSS
Pr2_ID02	08:13:17.9	+43:56:20.6	0.254	17.0	116.9	44.4	65.6	8.80	SDSS
Pr2_ID03	08:44:45.3	+76:53:09.6	0.131	16.3	71.2	44.1	44.1	7.99	SDSS
Pr2_ID04	08:48:53.1	+28:24:11.8	0.198	16.5	107.6	44.0	41.8	8.52	SDSS
Pr2_ID05	09:04:27.3	+37:43:57.5	0.198	17.3	72.7	44.2	50.3	7.79	SDSS
Pr2_ID06	09:36:08.7	+65:10:54.9	0.192	17.0	81.7	44.3	60.9	7.78	SDSS
Pr2_ID07	09:37:02.9	+68:24:08.4	0.295	15.8	258.3	44.2	55.0	8.35	SDSS
Pr2_ID08	10:56:09.8	+55:16:04.0	0.256	16.3	167.1	44.3	58.2	8.21	SDSS
Pr2_ID09	11:17:06.4	+44:13:33.3	0.144	16.1	89.8	44.3	56.3	8.58	SDSS
Pr2_ID10	11:18:30.3	+40:25:54.0	0.154	16.0	99.9	44.2	47.8	7.93	SDSS
Pr2_ID11	11:36:17.1	+44:10:22.6	0.198	17.2	76.3	44.2	50.3	8.60	SDSS
Pr2_ID12	11:52:53.5	+45:34:02.9	0.211	17.2	83.0	44.2	53.4	8.76	SDSS
Pr2_ID13	12:20:28.1	+40:50:35.0	0.222	16.3	138.6	44.3	62.4	8.81	SDSS
Pr2_ID14	12:28:30.9	+28:14:11.8	0.100	13.2	233.3	44.0	38.9	8.59	SDSS
Pr2_ID15	12:59:08.4	+56:15:30.7	0.161	17.2	58.6	44.2	51.2	8.80	SDSS
Pr2_ID16	13:05:16.8	+26:13:04.0	0.183	17.2	69.2	44.2	47.9	8.11	SDSS
Pr2_ID17	13:20:59.4	+29:57:28.1	0.206	17.2	80.7	44.4	67.1	8.80	SDSS
Pr2_ID18	13:23:49.5	+65:41:48.2	0.168	15.9	120.1	44.4	67.4	8.30	SDSS
Pr2_ID19	13:30:16.1	+52:51:01.9	0.162	16.4	87.9	44.3	56.5	8.91	SDSS
Pr2_ID20	14:05:02.6	+47:07:47.5	0.152	14.9	169.1	44.1	42.8	8.10	SDSS
Pr2_ID21	14:05:16.2	+25:55:34.2	0.164	15.6	133.6	44.3	54.6	8.04	SDSS
Pr2_ID22	14:06:21.9	+22:23:46.6	0.098	15.8	63.4	44.2	45.0	7.58	SDSS
Pr2_ID23	14:17:00.8	+44:56:06.6	0.114	15.7	78.3	44.2	46.8	7.97	SDSS
Pr2_ID24	14:29:43.1	+47:47:26.2	0.220	16.3	135.0	44.4	65.4	8.21	SDSS
Pr2_ID25	14:37:47.9	+28:30:19.5	0.249	17.2	104.2	44.1	48.7	8.58	SDSS
Pr2_ID26	14:42:07.5	+35:26:23.0	0.079	15.0	73.1	44.2	48.7	7.69	SDSS
Pr2_ID27	14:53:45.7	+34:33:20.3	0.209	17.2	81.9	44.2	51.4	8.75	SDSS
Pr2_ID28	15:21:14.3	+22:27:43.9	0.137	16.1	82.9	44.1	42.2	7.82	SDSS
Pr2_ID29	15:26:21.7	+43:23:49.6	0.156	16.3	88.5	44.0	39.4	7.82	SDSS
Pr2_ID30	15:33:54.7	+23:56:14.8	0.232	17.2	94.3	44.2	52.3	8.72	SDSS
Pr2_ID31	15:35:39.2	+56:44:06.5	0.207	16.8	98.3	44.3	60.2	9.08	SDSS
Pr2_ID32	15:42:34.8	+57:41:41.9	0.245	17.3	96.5	44.4	66.8	7.98	SDSS
Pr2_ID33	15:44:50.0	+43:51:51.3	0.149	16.9	61.6	44.1	41.1	8.76	SDSS
Pr2_ID34	16:05:07.9	+48:34:22.1	0.295	16.7	166.1	44.9	131.5	8.83	SDSS
Pr2_ID35	16:14:13.2	+26:04:16.3	0.131	16.0	82.5	44.4	62.2	8.26	SDSS
Pr2_ID36	16:25:33.8	+37:10:42.8	0.202	17.0	86.6	44.2	50.4	7.60	SDSS
Pr2_ID37	16:27:56.1	+55:22:31.5	0.133	16.2	76.7	44.4	63.8	8.45	BG92

Columns: (1) Target ID. (2) RA in J2000.0. (3) Dec in J2000.0 (4) Redshift. (5) Apparent B-band magnitude from the literature. (6) Observer-frame time lag $(1+z)\tau$ in days, estimated from the B-band magnitude in column (5). (7) L_{5100} measured from a reference spectrum. (8) $(1+z)\tau$ value measured using column (7) and Equation (3). (9) Black hole mass estimated using Equation (4) using the velocity dispersion (σ) of a broad Hβ emission line and L_{5100} in column (7). (10) References for individual spectra: SDSS – SDSS DR12 archive, BG92 – Boroson & Green (1992).

demonstrating the difficulty of time lag measurements for high-z targets due to, in average, fainter magnitude as well as the $(1+z)$ factor. For the continuum photometry monitoring, we will use the B-band filter for AGNs at $z < 0.3$ and the V-band filter for AGNs at higher z, considering the location of the Hβ emission line in the observed spectra. By proper choice of the photometric filter band we can largely – though not always, depending on the target redshift – avoid the variable Hβ emission line in our broad-band photometry.

To estimate the Hβ lag of each target, we calculate its optical luminosity using its apparent B-band magnitude. First, we calculate the absolute B-band magnitude (M_B) using a relation pointed out by Véron-Cetty & Véron (2010), assuming an optical spectral index $\alpha = 0.3$:

$$M_B = B + 5 - 5\log D - k + \Delta m(z) \quad (1)$$

where D is the luminosity distance, z is the redshift, $k = -2.5\log(1+z)^{1-\alpha}$ is the k-correction factor, and $\Delta m(z)$ is a correction to k which takes into account that the spectrum is not a power law (see Table 2 in Véron-Cetty & Véron (2010) for the values of $\Delta m(z)$ for $z < 5.0$). We then convert the absolute magnitude M_B into the luminosity at 5100 Å using Equation (2) in Marziani et al. (2003), assuming galactic extinction $A_B = 0$:

$$L_{5100} = 3.137 \times 10^{35-0.4M_B} \ \ (\mathrm{erg\ s^{-1}}) \quad (2)$$

Table 3
Properties of the AGNs from the Palomar Green catalog

Name	RA	Dec	z	B	$(1+z)\tau$ (day)	$\log L_{5100,spec}$ (erg s^{-1})	$(1+z)\tau_{\rm spec}$ (day)	$\log M_{\rm BH}$ ($M_\odot$)	Ref. Spec.
(1)	(2)	(3)	(4)	(5)	(6)	(7)	(8)	(9)	(10)
P01	00:05:59.2	+16:09:49.0	0.451	16.0	455.8	45.6	331.2	9.48	BG92
P02	00:10:31.0	+10:58:29.5	0.089	16.1	49.2	44.4	57.0	8.74	BG92
P03	00:29:13.7	+13:16:04.0	0.142	15.0	159.6	44.6	79.3	8.61	BG92
P04	00:45:47.2	+04:10:23.3	0.385	15.9	370.9	45.2	213.5	8.81	BG92
P05	00:53:34.9	+12:41:35.9	0.059	14.4	70.0	44.3	49.6	7.92	BG92
P06	00:54:52.1	+25:25:39.0	0.154	15.4	142.6	44.7	90.6	9.06	BG92
P07	01:59:50.3	+00:23:40.8	0.163	15.2	160.5	44.6	76.9	9.23	BG92
P08	21:14:52.6	+06:07:42.5	0.466	15.5	595.8	45.6	338.8	9.29	BG92
P09	21:32:27.8	+10:08:19.2	0.063	14.9	66.9	44.3	50.4	8.14	BG92
P10	22:11:53.9	+18:41:50.0	0.070	15.9	41.7	43.6	23.1	8.44	BG92
P11	22:17:12.3	+14:14:20.9	0.066	15.0	60.1	44.4	55.1	8.35	BG92
P12	22:36:07.7	+13:43:55.4	0.326	16.0	267.7	45.0	148.6	8.32	BG92
P13	22:54:10.4	+11:36:38.7	0.326	16.3	239.7	45.5	281.2	9.23	BG92
P14	23:11:17.8	+10:08:15.8	0.433	16.1	398.1	45.2	218.2	9.50	BG92
P15	23:51:56.1	-01:09:13.3	0.174	15.0	190.1	44.6	84.6	8.98	Lick

Columns: (1) Target ID. (2) RA in J2000.0. (3) Dec in J2000.0 (4) Redshift. (5) Apparent B-band magnitude from the literature. (6) Observer-frame time lag $(1+z)\tau$ in days, estimated from the B-band magnitude in column (5). (7) L_{5100} measured from a reference spectrum. (8) $(1+z)\tau$ value measured using column (7) and Equation (3). (9) Black hole mass estimated using Equation (4) using the velocity dispersion (σ) of a broad Hβ emission line and L_{5100} in column (7). (10) References for individual spectra: BG92 – Boroson & Green (1992), Lick – obtained with our program.

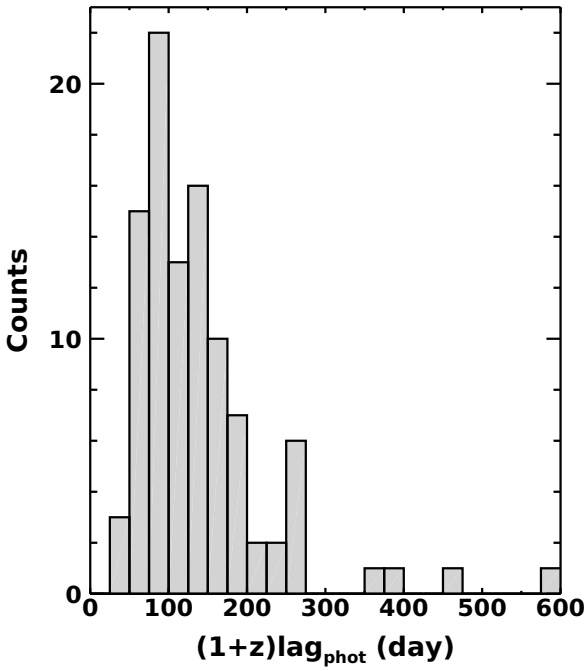

Figure 7. Distribution of expected observer-frame time lags calculated from the monochromatic luminosity at 5100 Å obtained from broad-band photometry.

Using this photometric estimate of L_{5100}, we calculate the Hβ lag, using the size-luminosity relation of Bentz et al. (2013),

$$\log\left(\frac{c\tau}{\text{light day}}\right) = 1.527 + 0.533\log\left(\frac{L_{5100}}{10^{44}\text{erg s}^{-1}}\right) \quad (3)$$

where c is the speed of light. The time lags τ expected for our targets are given in Tables 1–3. In Figure 7, we show the distribution of the expected Hβ lags, ranging from 42 to 596 days with a mean of 140 ± 87 days. As expected, the majority of targets have Hβ lags around 100–300 days, while a small fraction of the sample has a larger lag of over 300 days. Note that the estimated lags are quite uncertain due to the transformation from broad-band photometry.

In order to measure AGN properties and estimate the Hβ lag from the luminosity at 5100 Å, we analyze the spectrum of each target. The raw spectra have been compiled from the SDSS DR12 archive for targets listed in the MILLIQUAS Catalog while we also used the NED database for the PG quasars (Boroson & Green 1992). We perform spectral decomposition to separate out the AGN continuum by following the procedure given in previous studies (Woo et al. 2006; Park et al. 2012; Woo et al. 2015). We use three main components to fit the continuum: a power-law component representing the featureless AGN continuum, a Fe II template from Boroson & Green (1992) to fit the Fe II emission blends, and a stellar population model that takes into account the host galaxy star light. We work on the spectral ranges 4430–4600 Å and 5080–5550 Å where Fe II emission blends dominate. For the multi-component analysis, we use the nonlinear Levenberg-Marquardt least-squares fitting routine `mpfit` (Markwardt 2009) in IDL. In Figure 8, we demonstrate the fitting procedure for three examples. Based on the best-fit results, we also determine the monochromatic luminosity at 5100 Å from the power-law component.

In Figure 9, we present the Hβ lags estimated from the measured L_{5100}. The mean lag of the sample is 90 days with a standard deviation of 58 days. The

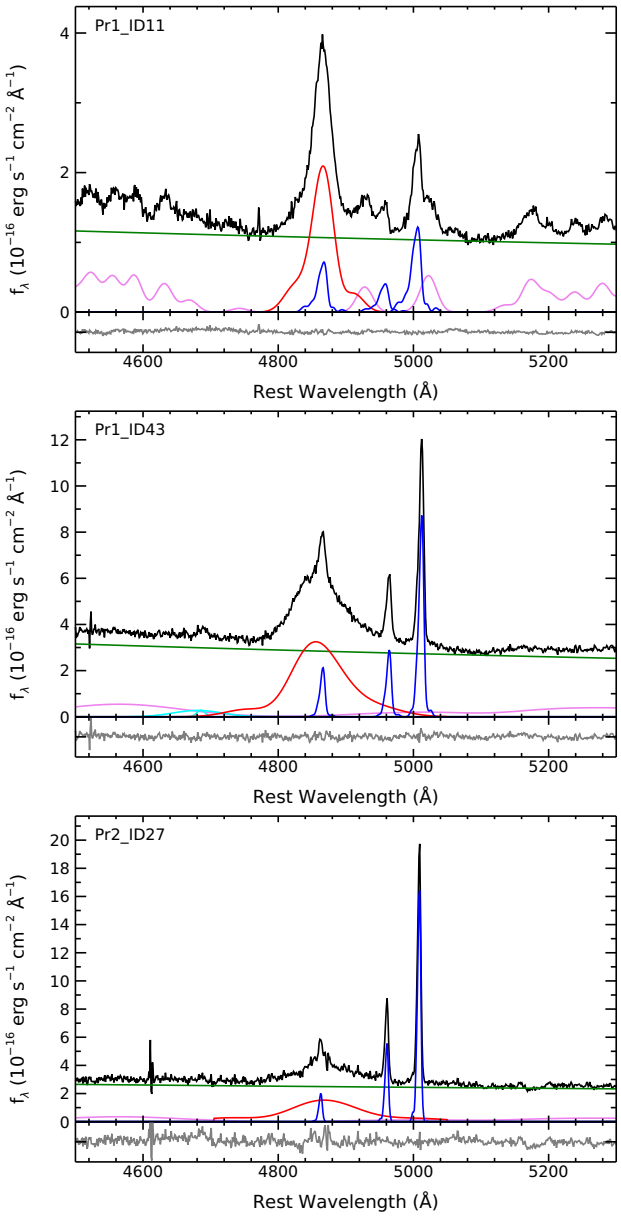

Figure 8. Examples of spectral decomposition for three targets. The observed spectrum (black) is fitted with three components: a power-law (green), Fe II emission blends (magenta), and a stellar population model. Note that since stellar flux is weak, the stellar component is negligible in the fit. The broad Hβ (red) as well as narrow Hβ and O III lines (blue) are fitted separately.

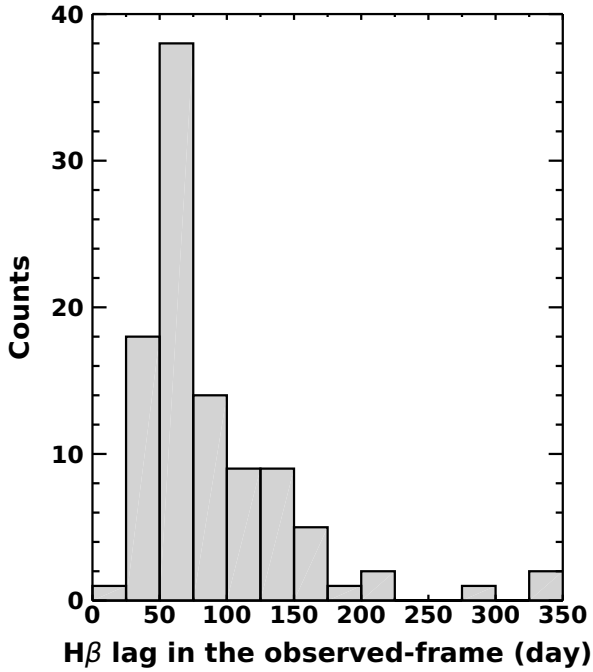

Figure 9. Distribution of expected observer-frame time lags calculated from the monochromatic luminosity at 5100 Å from the spectral decomposition analysis.

Hβ lag derived from spectroscopy is somewhat different from the one derived from photometry (see Figure 10), reflecting the uncertainty in the transformation of the broad band magnitude to the monochromatic luminosity at 5100 Å and temporal variability as photometry and spectroscopy were not simultaneous. Since L_{5100} is a directly measured monochromatic luminosity at 5100 Å, the Hβ lag based on spectroscopy is more appropriate to use for designing our monitoring campaign. Even for the spectroscopy-based Hβ lags, there are a number of uncertainties, including the flux uncertainty from spectrophotometric calibration, a systematic uncertainty in separating AGN continuum from the stellar component and Fe II emission, and the intrinsic scatter in the size-luminosity relation. Moreover, as the variability of an AGN will change the optical luminosity and the Hβ lag as a function of time, the estimated lag should be used only as an initial estimate, and the true Hβ lag should be measured from cross correlation analysis.

We determine the $M_{\rm BH}$ of each target using L_{5100} and the line dispersion of the Hβ line, $\sigma_{\rm H\beta}$, from the relation

$$M_{\rm BH} = f_{\rm v} \times 10^{6.819} \left(\frac{\sigma_{\rm H\beta}}{10^3\,{\rm km\,s^{-1}}}\right)^2 \left(\frac{\lambda L_{5100}}{10^{44}\,{\rm erg\,s^{-1}}}\right)^{0.533} M_\odot \quad (4)$$

where the $f_{\rm v}$ is the virial factor which has been determined empirically from the $M_{\rm BH}$–stellar velocity dispersion relation by Woo et al. (2015). While we will measure the Hβ lag and determine the reverberation-based $M_{\rm BH}$, the estimated mass enables us to investigate the properties of the sample although there are large uncertainties. In Figure 11, we compare the derived $M_{\rm BH}$ with bolometric AGN luminosity, which is calculated by multiplying a factor of 10 to L_{5100} (Woo & Urry 2002). The $M_{\rm BH}$ of the sample ranges from $\log M_{\rm BH} = 7.3$ to 9.5 and the Eddington ratio ranges from 1% to close to 100%, indicating that the sample contains intermediate to high-Eddington AGNs.

5. Summary and Conclusions

To overcome the current limitations of reverberation studies, which have mainly focused on relatively low-

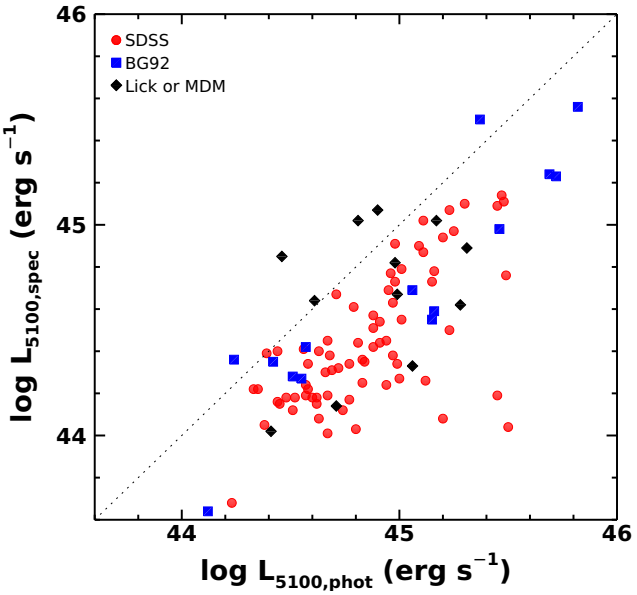

Figure 10. Comparison of the luminosity at 5100 Å between the estimates based on the broad-band photometry and the measurements from the spectral decomposition analysis. Symbol identify the sources of the reference spectra: SDSS (red dots), Boroson & Green (1992) (blue squares), Lick 3-m or MDM 2.4-m (black diamonds).

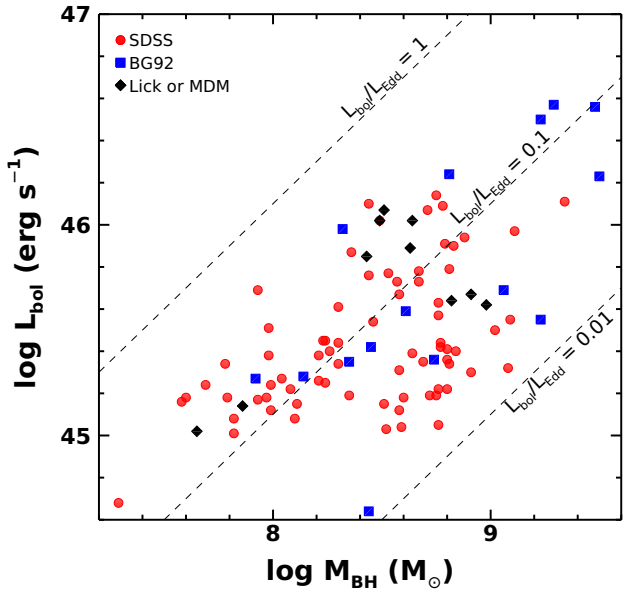

Figure 11. Distributions of $M_{\rm BH}$ and bolometric luminosity. Specific Eddington ratios are marked by dashed lines. Symbols are as in Figure 10.

to-moderate luminosity AGNs at low redshift, we developed a new reverberation mapping project, aiming at measuring Hβ lags for relatively luminous AGNs out to z$\sim$0.5. We described the strategy of the Seoul National University AGN Monitoring Project, which was designed to be carried out over three years. We performed simulations to generate light curves and measured the success rate for the lag measurements using various sets of parameters, including campaign duration, time cadence, seasonal gaps, and variability characteristics. Based on the simulation results and the availability of telescope time, we determined the optimal cadence and sample parameters for a three year monitoring project.

While reverberation mapping for high-z AGNs is much more challenging due to the large $(1+z)$ factor, requiring a factor of $(1+z)$ longer monitoring campaign, the recent C IV lag measurements from a long-term campaign clearly showed the feasibility (Lira et al. 2018). However, in order to study the Hβ size-luminosity relation with very luminous AGNs at high z, a monitoring campaign with infrared spectroscopy is required due to the redshift of the Hβ emission line, which is much more challenging.

We selected a sample of 100 AGNs for the project, and described the photometric and spectroscopic properties using archival data. The expected lag based on the monochromatic luminosity at 5100 Å ranges between 40 and $\sim$350 days, which can be measured with a three year monitoring project. As the sample covers high luminosity and high Eddington ratio AGNs at higher redshift than the local reverberation sample, we expect that the size-luminosity relation will be tested in the high-luminosity regime, which is relevant for measuring the $M_{\rm BH}$ of high-z QSOs.

ACKNOWLEDGMENTS

We thank the anonymous referees for their comments, which improved the clarity of the manuscript. This work was supported by the Samsung Science and Technology Foundation under Project Number SSTF-BA1501-05 and the National Research Foundation of Korea grant funded by the Korean government (No. 2016R1A2B3011457).

REFERENCES

Barth, A. J., Pancoast, A., Thorman, S. J., et al. 2011, The Lick AGN Monitoring Project 2011: Reverberation Mapping of Markarian 50, ApJL, 743, L4

Barth, A. J., Bennert, V. N., Canalizo, G., et al. 2015, The Lick AGN Monitoring Project 2011: Spectroscopic Campaign and Emission-line Light Curves, ApJS, 217, 26

Bentz, M. C., Peterson, B. M., Pogge, R. W., Vestergaard, M., & Onken, C. A. 2006, The Radius-Luminosity Relationship for Active Galactic Nuclei: The Effect of Host-Galaxy Starlight on Luminosity Measurements, ApJ, 644, 133

Bentz, M. C., Peterson, B. M., Netzer, H., Pogge, R. W., & Vestergaard, M. 2009, The Radius-Luminosity Relationship for Active Galactic Nuclei: The Effect of Host-Galaxy Starlight on Luminosity Measurements. II. The Full Sample of Reverberation-Mapped AGNs, ApJ, 697, 160

Bentz, M. C., Horne, K., Barth, A. J., et al. 2010, The Lick AGN Monitoring Project: Velocity-delay Maps from the Maximum-entropy Method for Arp 151, ApJ, 720, L46

Bentz, M. C., Denney, K. D., Grier, C. J., et al. 2013, The Low-luminosity End of the Radius-Luminosity Relationship for Active Galactic Nuclei, ApJ, 767, 149

Blandford, R. D., & McKee, C. F. 1982, Reverberation Mapping of the Emission Line Regions of Seyfert Galaxies and Quasars, ApJ, 255, 419
Boroson, T. A., & Green, R. F. 1992, The Emission-line Properties of Low-redshift Quasi-stellar Objects, ApJS, 80, 109
Davis, S. W., Woo, J.-H., & Blaes, O. M. 2007, The UV Continuum of Quasars: Models and SDSS Spectral Slopes, ApJ, 668, 682
Du, P., Hu, C., Lu, K.-X., et al. 2015, Supermassive Black Holes with High Accretion Rates in Active Galactic Nuclei. IV. Hβ Time Lags and Implications for Super-Eddington Accretion, ApJ, 806, 22
Du, P., Lu, K.-X., Zhang, Z.-X., et al. 2016, Supermassive Black Holes with High Accretion Rates in Active Galactic Nuclei. V. A New Size-Luminosity Scaling Relation for the Broad-line Region, ApJ, 825, 126
Fausnaugh, M. M., Grier, C. J., Bentz, M. C., et al. 2017, Reverberation Mapping of Optical Emission Lines in Five Active Galaxies, ApJ, 840, 97
Ferrarese, L., & Merritt, D. 2000, A Fundamental Relation between Supermassive Black Holes and Their Host Galaxies, ApJL, 539, L9
Gebhardt, K., Bender, R., Bower, G., et al. 2000, A Relationship between Nuclear Black Hole Mass and Galaxy Velocity Dispersion, ApJL, 539, L13
Grier, C. J., Martini, P., Watson, L. C., et al. 2013, Stellar Velocity Dispersion Measurements in High-luminosity Quasar Hosts and Implications for the AGN Black Hole Mass Scale, ApJ, 773, 90
Grier, C. J., Trump, J. R., Shen, Y., et al. 2017, The Sloan Digital Sky Survey Reverberation Mapping Project: Hα and Hβ Reverberation Measurements from First-year Spectroscopy and Photometry, ApJ, 851, 21
Kaspi, S., Smith, P. S., Netzer, H., et al. 2000, Reverberation Measurements for 17 Quasars and the Size–Mass–Luminosity Relations in Active Galactic Nuclei, ApJ, 533, 631
Kollmeier, J. A., Onken, C. A., Kochanek, C. S., et al. 2006, Black Hole Masses and Eddington Ratios at $0.3 < z < 4$, ApJ, 648, 128
Kormendy, J., & Ho, L. C. 2013, Coevolution (Or Not) of Supermassive Black Holes and Host Galaxies, ARA&A, 51, 511
Lawrence, A., Saunders, W., Rowan-Robinson, M., et al. 1988, Extreme Fe II Emission from an IRAS Quasar, MNRAS, 235, 261
Lira, P., Kaspi, S., Netzer, H., et al. 2018, Reverberation Mapping of Luminous Quasars at High z, ApJ, 865, 56
Markwardt, C. B. 2009, Non-linear Least-squares Fitting in IDL with MPFIT, in Astronomical Society of the Pacific Conference Series, Vol. 411, Astronomical Data Analysis Software and Systems XVIII, ed. D. A. Bohlender, D. Durand, & P. Dowler, 251
Marziani, P., Zamanov, R. K., Sulentic, J. W., & Calvani, M. 2003, Searching for the Physical Drivers of Eigenvector 1: Influence of Black Hole Mass and Eddington Ratio, MNRAS, 345, 1133
Park, D., Woo, J.-H., Treu, T., et al. 2012, The Lick AGN Monitoring Project: Recalibrating Single-epoch Virial Black Hole Mass Estimates, ApJ, 747, 30
Park, S., Woo, J.-H., Romero-Colmenero, E., et al. 2017, Reverberation Mapping of PG 0934+013 with the Southern African Large Telescope, ApJ, 847, 125
Pancoast, A., Brewer, B. J., Treu, T., et al. 2014, Modelling Reverberation Mapping Data – II. Dynamical modelling of the Lick AGN Monitoring Project 2008 data set, MNRAS, 445, 3073
Peterson, B. M. 1993, Reverberation Mapping of Active Galactic Nuclei, PASP, 105, 247
Peterson, B. M., Ferrarese, L., Gilbert, K. M., et al. 2004, Central Masses and Broad-Line Region Sizes of Active Galactic Nuclei. II. A Homogeneous Analysis of a Large Reverberation-Mapping Database, ApJ, 613, 682
Rakshit, S., Woo, J.-H., Gallo, E., et al. 2019, The Seoul National University AGN Monitoring Project. II. BLR Size and Black Hole Mass of Two AGNs, ApJ, submitted
Shen, Y., Horne, K., Grier, C. J., et al. 2016, The Sloan Digital Sky Survey Reverberation Mapping Project: First Broad-line Hβ and Mg II Lags at $z \geq 0.3$ from Six-month Spectroscopy, ApJ, 818, 30
Timmer, J., & König, M. 1995, On Generating Power Law Noise, A&A, 300, 707
Véron-Cetty, M.-P. & Véron, P. 2010, A Catalogue of Quasars and Active Galactic Nuclei: 13th Edition, A&A, 518, A10
Wandel, A., Peterson, B. M., & Malkan, M. A. 1999, Central Masses and Broad-Line Region Sizes of Active Galactic Nuclei. I. Comparing the Photoionization and Reverberation Techniques, ApJ, 526, 579
Woo, J.-H., & Urry, C. M. 2002, Active Galactic Nucleus Black Hole Masses and Bolometric Luminosities, ApJ, 579, 530
Woo, J.-H., Treu, T., Malkan, M. A., & Blandford, R. D. 2006, Cosmic Evolution of Black Holes and Spheroids. I. The $M_{\rm BH}$–σ_* Relation at $z = 0.36$, ApJ, 645, 900
Woo, J.-H., Schulze, A., Park, D., et al. 2013, Do Quiescent and Active Galaxies Have Different $M_{\rm BH}$–σ_* Relations?, ApJ, 772, 49
Woo, J.-H., Yoon, Y., Park, S., et al. 2015, The Black Hole Mass-Stellar Velocity Dispersion Relation of Narrow-line Seyfert 1 Galaxies, ApJ, 801, 38
Woo, J.-H., Bae, H.-J., Son, D., & Karouzos, M. 2016, The Prevalence of Gas Outflows in Type 2 AGNs, ApJ, 817, 108
Zu, Y., Kochanek, C. S., & Peterson, B. M. 2011, An Alternative Approach to Measuring Reverberation Lags in Active Galactic Nuclei, ApJ, 735, 80
Zu, Y., Kochanek, C. S., Kozłowski, S., & Udalski, A. 2013, Is Quasar Optical Variability a Damped Random Walk?, ApJ, 765, 106